First principles hybrid Hartree–Fock–DFT calculations of bulk and (001) surface *F* centers in oxide perovskites and alkaline-earth fluorides

R. Eglitis[1], A. I. Popov[1], J. Purans[1], and Ran Jia[1,2]

[1]Institute of Solid State Physics, University of Latvia, Riga LV-1063, Latvia

[2]Laboratory of Theoretical and Computational Chemistry, Institute of Theoretical Chemistry, Jilin University
Changchun 130023, PR China
E-mail: rieglitis@gmail.com
popov@latnet.lv

We report the results of *ab initio* calculations and analysis of systematic trends for the *F* centers in the bulk and on the (001) surface in oxide perovskites, such as $BaTiO_3$, $SrTiO_3$, $SrZrO_3$, and $PbZrO_3$, with a corresponding comparison of the *F* centers in perovskites with those in alkaline earth metal fluorides (CaF_2, BaF_2, and SrF_2). It was found that in perovskites in both bulk *F* centers and those on their (001) surfaces, two nearest to the vacancy Ti or Zr atoms repel each other, while the next nearest O atoms relax towards the oxygen vacancy. It was also found that the obtained relaxations of atoms in the nearest neighborhood around the *F* center in ABO_3 perovskites are generally larger than in alkaline earth metal fluorides. The bulk and (001)-terminated surface *F* center ground states in $BaTiO_3$, $SrTiO_3$, and $SrZrO_3$ perovskites are located 0.23, 0.69, 1.12 eV, and 0.07, 0.25, 0.93 eV, respectively, below the conduction band bottom, indicating that the *F* center is a shallow donor. The vacancies in $BaTiO_3$, $SrZrO_3$, and $PbZrO_3$ are occupied with $1.103e$, $1.25e$, and $0.68e$, respectively, whereas slightly smaller charges, only $1.052e$, $1.10e$, and $0.3e$ are localized inside the *F* center on the perovskite (001) surface. In contrast to the partly covalent ABO_3 perovskites, charge is well localized (around 80 %) inside the ionic CaF_2, BaF_2, and SrF_2 fluorine vacancy.

Keywords: *Ab initio* calculations, *F* center, perovskites.

1. Introduction

Point defects, such as oxygen vacancies, significantly affect all the physical and chemical properties of the industrially important ABO_3 perovskites [1–7]. Renewed interest in comprehensive research of point-defective behavior in oxide perovskite materials is due to their possible use as electronic conductors [8], an active component in all-oxide electronics [9], memristive elements [10] and *etc.* [11–13]. The oxygen vacancy is quite a common defect in many binary and complex oxide materials [14–27]. They can be created, when irradiated with high energy particles [18–19] or during the thermochemical reduction processes [20–21]. As usual, these oxygen vacancies effectively capture electrons and become either neutral or positively charged with respect to the lattice (the so-called *F* centers or F^+ centers, respectively [22–27]).

The *F* centers are formed in oxide perovskites when neutral O atoms removed from the regular lattice sites. Such point defects strongly affect and perturb the electronic structure of the crystal and it becomes essentially more complex for oxygen-deficient perovskite material than a perfect crystal.

Compared to simple alkali halides, alkaline-earth halides, MgF_2 or LaF_3 [19, 28–31] and binary simple oxides such as MgO or Al_2O_3 [18, 19], the more complex electronic structure of oxide perovkites has important implications for the electronic structure of the corresponding *F*-type centers [18, 19, 22, 24]. In ionic oxides, the ground state of the *F* center contains two electrons, which are well localized in vacancies, which leads to the appearance of energy levels in the band gap [19], while for perovskite oxides, the electronic structure of *F*-type defects has been the subject of long discussions [16–19, 22, 24]. It is very important to notice, that most of the theoretical and experimental work in the ABO_3 perovskites are performed for the bulk *F* centers [16–19, 22, 24–38]. Unfortunately, the BO_2 and especially AO-terminated (001) surface *F* centers in the ABO_3 perovskites are considerably less studied [39–45].

The *F* centers created and stabilized on the surface, along with other anionic defects, are also important in catalysis [46, 47]. It has been reported, for example, that the surface *F* center in NaCl binds strongly to sodium adatom and increases the binding energy by 1 eV, changing the nature of adsorption of a single sodium adatom from physical sorption to chemisorption [48]. However, not many experimental results regarding the properties of the surface color center are up to now available, where there is often no clear and unambiguous separation from the contributions of bulk defects [49–51] Other studies that focused on desorbed particles from ionic crystals under photon or electron bombardment, provide only indirect information about the created surface defects [52–53]. Using a combination of low-energy electron diffraction and energy loss spectroscopy, it was a big breakthrough to study the formation of defects in epitaxial NaCl films with a thickness of the order of several nm at low energies of ~ 50–1500 eV electron bombardment [54]. In the light of the above, it is especially important to note the use of synchrotron radiation for studying of *F* centers at the surface of epitaxial CaF$_2$ films on Si (111) [55].

Taking into account the high technological potential of alkaline-earth fluorites (CaF$_2$, BaF$_2$, and SrF$_2$), it is obvious, that during the last years, they were widely studied both experimentally and theoretically [55–63]. Fluorites CaF$_2$, BaF$_2$, and SrF$_2$ are a cubic *Fm3m* large band gap insulators. For example, experimentally, the CaF$_2$ direct band gap is estimated to be 12.1 eV [64], whereas the CaF$_2$ indirect band gap is equal to 11.8 eV [64]. On the other hand, the band gap energies and the positions of the absorption band maxima for the main V_k, *H*, and *F*-type defects in fluorides were recently analysed and collected in [65]. In particular, for band gap energies E_g in CaF$_2$, SrF$_2$, and BaF$_2$, the following values were given as 11.5, 10.8, and 10.3 eV, respectively. The corresponding values of the optical absorption energy for bulk *F* centers in these crystals are as follows 3.35, 2.76, and 2.04 eV, respectively [65]. Note that the corresponding reliable values for surface *F* centers in fluorides are currently not available.

The main goal of the research work reported here was to develop a unified theory, which describes systematic trends in the ABO$_3$ perovskite bulk and rarely studied (001) surface *F* center calculations. We also compared our *F* center calculation results in the ABO$_3$ perovskites as well as CaF$_2$, BaF$_2$, and SrF$_2$ crystals, and pointed out quite different behavior of the *F* centers in this two different class of materials.

2. Method

We performed *ab initio* calculations for BaTiO$_3$, SrZrO$_3$, and PbZrO$_3$ perovskite bulk as well as (001) surface *F* centers [2, 41, 43, 46] using the hybrid exchange-correlation functionals B3PW [66] or B3LYP [67] as well as the world widely recognized CRYSTAL computer code [68]. The results of SrTiO$_3$ bulk and TiO$_2$-terminated (001)
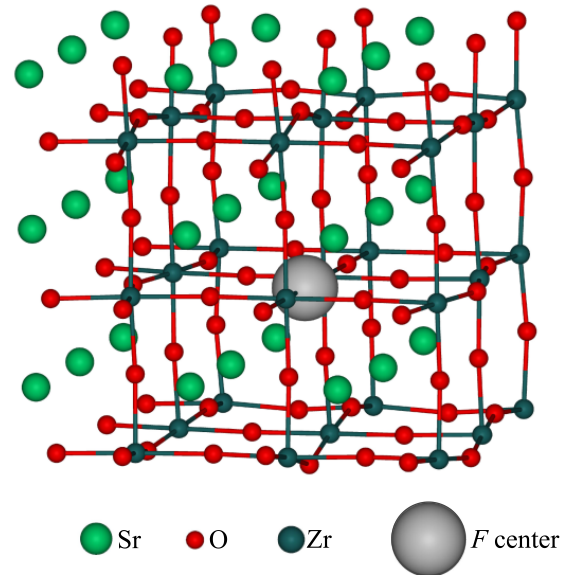
Fig. 1. Schematic sketch of the cubic $3 \times 3 \times 3$ times extended SrZrO$_3$ supercell containing the *F* center.

surface *F* centers for comparison purpose are listed from the Ref. 22. We carried out the SrZrO$_3$, PbZrO$_3$, and BaTiO$_3$ bulk *F* center calculations using the $3 \times 3 \times 3$ times extended supercell model (Fig. 1). Thereby, our in the calculations used supercell contains 134 atoms as well as one isolated oxygen vacancy defect (*F* center) (Fig. 1). We calculated the formation energy of a single *F* center defect in the BaTiO$_3$, SrZrO$_3$, and PbZrO$_3$ bulk using the following equation:

$$E_{\text{form}} = E_{\text{oxy}} + E_F - E_{\text{perf}}, \qquad (1)$$

where E_{oxy} is our calculated single oxygen atom total energy. E_{perf} is our calculated perfect BaTiO$_3$, SrZrO$_3$ or PbZrO$_3$ perovskite bulk total energies. E_F is the total energy for the BaTiO$_3$, SrZrO$_3$ or PbZrO$_3$ perovskite bulk containing the *F* center defect.

For the *ab initio* calculations of the (001) surface *F* centers in BaTiO$_3$, SrZrO$_3$, and PbZrO$_3$ perovskites, we always have used a $3 \times 3 \times 1$ times extended surface supercells and removed only one atom, namely the central (001) surface O atom (Fig. 2). We calculated the *F* center located on the ZrO$_2$-terminated SrZrO$_3$ (Fig. 2) and PbZrO$_3$ as well as BaO-terminated BaTiO$_3$ (001) surfaces. Thereby, the SrZrO$_3$ and PbZrO$_3$ ZrO$_2$-terminated (001) surface *F* center concentration in our calculations is equal to 1/18 or 5.56 %. In order to perform more accurate calculations of the bulk and (001) surface *F* centers in BaTiO$_3$, SrZrO$_3$, and PbZrO$_3$ perovskites, an additional basis function, corresponding to the so called ghost atom [68], has been put into the oxygen vacancy. For this aim, we have employed, in our *ab initio* calculations, exactly the same Gaussian-type functions as used by us for the O^{2-} ions in the bulk of BaTiO$_3$, SrZrO$_3$, and PbZrO$_3$ perovskites.
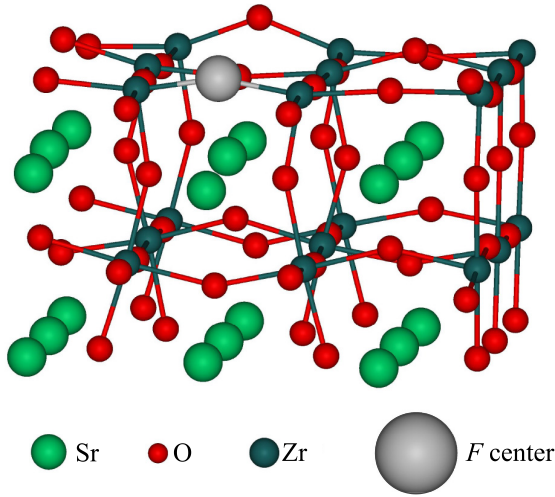
Fig. 2. Sketch of the *F* center located on the ZrO_2-terminated $SrZrO_3$ (001) surface.

As a next point, we will discuss our calculations dealing with the bulk *F* centers in CaF_2, BaF_2, and SrF_2 crystals (Fig. 3). For example, in order to calculate the *F* centers in CaF_2, we used the supercell containing 48 atoms with one removed fluorine atom. After the removal of the single fluorine atom, we reoptimized the atomic structure of the defect surrounding atoms through the search of the minimum of the total energy as a function of the displacements of the atoms from their equilibrium lattice sites. Again, in order to have the perfect description of the *F* center, we added the basis set in the fluorine vacancy, corresponding to the so-called ghost atom [68].
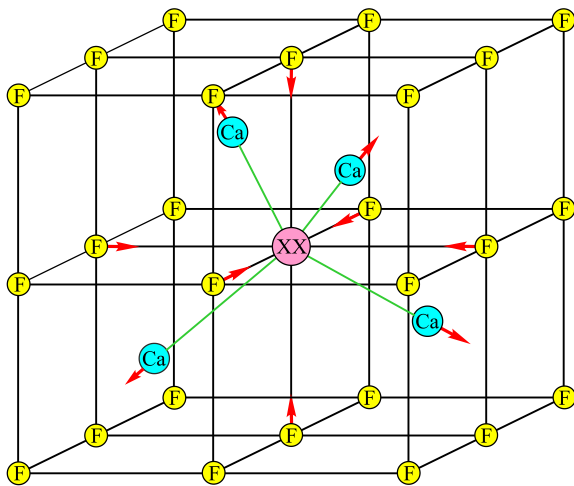
Fig. 3. Sketch of the nearest neighbor geometry around the *F* center in CaF_2 with the indication of atomic relaxation directions. The position of the *F* center is indicated by *XX*.

3. Main results

3.1. Atomic structure of bulk and (001) surface F centers in BaTiO₃, SrTiO₃, SrZrO₃, *and* PbZrO₃

As a starting point of our *ab initio* calculations, we calculated the nearest neighbor atom displacements surrounding the *F* centers in $BaTiO_3$, $SrZrO_3$, and $PbZrO_3$ bulk as well as on their BaO and ZrO_2-terminated (001) surfaces, respectively. Calculated nearest atom displacements surrounding the *F* centers in $BaTiO_3$, $SrZrO_3$, and $PbZrO_3$ bulk as well as on their (001) surfaces are collected by us in Table 1. As it is possible to see from Table 1, the two nearest to the *F* center in $BaTiO_3$ matrix Ti atoms are repulsed from the oxygen vacancy by 1.06 % of the lattice constant *a*. Also in $SrTiO_3$, $SrZrO_3$, and $PbZrO_3$ perovskites, the B atoms are repulsed from the *F* center by 7.76, 3.68, and 0.48 % of *a*. Just opposite, the second nearest neighbor O atoms in the $BaTiO_3$, $SrTiO_3$, and $SrZrO_3$ perovskites are always attracted towards the oxygen vacancy by 0.71, 7.79, and 2.63 % of the *a* (Table 1).

Qualitatively similar relaxation pattern, but with much larger atomic displacements than in the bulk *F* center cases is calculated also for the BO_2-terminated $SrTiO_3$, $SrZrO_3$, and $PbZrO_3$ as well as AO-terminated $BaTiO_3$ (001) surface *F* centers (Table 1). For example, the B atoms are repulsed from the (001) surface *F* centers located on the BO_2-terminated $SrTiO_3$, $SrZrO_3$, and $PbZrO_3$ (001) surfaces by 14, 9.17, and 8.46 % of the lattice constant *a*, respectively. In contrast, the second nearest neighbor O atoms are

Table 1. *Ab initio* B3PW calculated three nearest neighbor atom displacements around the bulk as well as (001) surface *F* centers in $BaTiO_3$, $SrTiO_3$, $SrZrO_3$, and $PbZrO_3$ perovskites. All atomic displacements are in percents of the calculated lattice constant *a*

	BaTiO₃	SrTiO₃	SrZrO₃	PbZrO₃
Lattice constant, Å	4.007	3.904	4.163	4.177
Bulk *F* center				
B relax., % of *a*	1.06	7.76	3.68	0.48
O relax., % of *a*	−0.71	−7.79	−2.63	–
A relax., % of *a*	−0.08	3.94	0.46	−5.99
F center on (001) surface				
B relax., % of *a*	0.1	14	9.17	8.46
O relax., % of *a*	−1.4	−8	−4.16	–
A relax., % of *a*	1.0	–	7.68	11.97

attracted towards the surface F centers on the BO_2 as well as AO-terminated (001) surfaces of $SrTiO_3$, $SrZrO_3$, and $BaTiO_3$ perovskites by slightly larger displacement magnitudes (8, 4.16, and 1.4 % of *a*) than in the bulk F center cases (Table 1).

3.2. Electronic structure of bulk and (001) surface F centers in BaTiO₃, SrTiO₃, SrZrO₃, and PbZrO₃

Inside the bulk F center, or in another words oxygen vacancy, in the $BaTiO_3$, $SrTiO_3$, $SrZrO_3$, and $PbZrO_3$ perovskites are located -1.103, -1.10, -1.25, and -0.68 electrons of additional charge. The *ab initio* calculated bulk F center formation energies for the $BaTiO_3$ (10.3 eV), $SrTiO_3$ (7.1 eV), $SrZrO_3$ (7.55 eV), and $PbZrO_3$ (7.25 eV) perovskites are in the energy range between 7.1 and 10.3 eV (Table 2 and Fig. 4). The bulk F center defect induce defect level in the band gap of ABO_3 perovskites (Fig. 5). The inside band gap induced defect levels in the ABO_3 perovskites are located closer to the conduction band bottom, than the valence band top. For example, in the $BaTiO_3$, $SrTiO_3$, $SrZrO_3$, and $PbZrO_3$ perovskite bulk, the F center induced defect levels are located 0.23, 0.69, 1.12, and 1.72 eV below the conduction band bottom (Table 2 and Fig. 5).

The charge inside the (001) surface F centers always are slightly more delocalized than inside the bulk F centers in the $BaTiO_3$, $SrZrO_3$, and $PbZrO_3$ perovskite matrixes (Table 2). Namely, there are only $-1.052e$, $-1.10e$, and $-0.3e$ localized inside the $BaTiO_3$, $SrZrO_3$, and $PbZrO_3$ (001) surface F centers (Table 2). The *ab initio* calculated oxygen vacancy formation energies on the $BaTiO_3$, $SrTiO_3$, $SrZrO_3$, and $PbZrO_3$ (001) surfaces are equal to 10.2, 6.22, 7.52, and 6.0 eV, respectively (Table 2). The calculated comparative formation energies of the bulk and (001) surface F centers

Table 2. *Ab initio* B3PW calculated electronic structure of the bulk as well as (001) surface F centers in $BaTiO_3$, $SrTiO_3$, $SrZrO_3$, and $PbZrO_3$ perovskites

	BaTiO₃	SrTiO₃	SrZrO₃	PbZrO₃
Bulk *F* center				
F center charge	$-1.103e$	$-1.10e$	$-1.25e$	$-0.68e$
F under conduction band, eV	0.23	0.69	1.12	1.72
E_{form}, eV	10.3	7.1	7.55	7.25
F center on (001) surface				
F center charge	$-1.052e$	–	$-1.10e$	$-0.3e$
F under conduction band, eV	0.07	0.25	0.93	2.58
E_{form}, eV	10.2	6.22	7.52	6.0
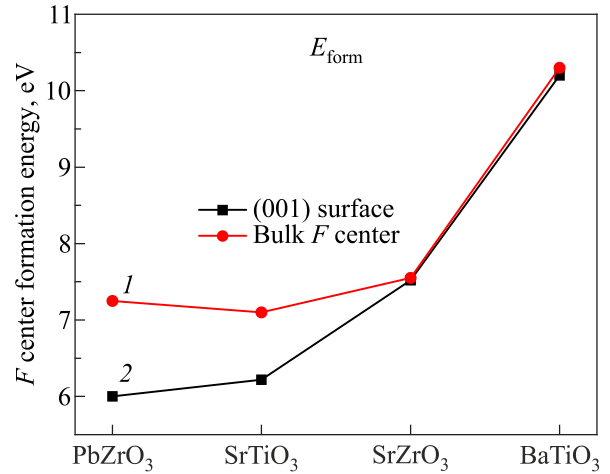
Fig. 4. Our *ab initio* calculated F center formation energy E_{form}, eV in the $PbZrO_3$, $SrTiO_3$, $SrZrO_3$, and $BaTiO_3$ perovskite bulk (*1*) and on their (001) surfaces (*2*).

in $BaTiO_3$, $SrTiO_3$, $SrZrO_3$, and $PbZrO_3$ perovskite matrixes are depicted in Fig. 4. The appropriate *ab initio* calculated F center induced defect levels for $BaTiO_3$, $SrTiO_3$, $SrZrO_3$, and $PbZrO_3$ perovskite (001) surfaces are located 0.07, 0.25, 0.93, and 2.58 eV, respectively, below the bottom of conduction band (Table 2, Fig. 5).

3.3. Ab initio calculations of the atomic and electronic structure of the bulk F centers in CaF₂, BaF₂, and SrF₂

As a starting point of our F center calculations in CaF_2, BaF_2, and SrF_2 crystals, we calculated the perfect CaF_2, BaF_2, and SrF_2 bulk lattice constant and compared them with the available experimental data. Our B3PW calculated bulk lattice constants for CaF_2 (5.50 Å), BaF_2 (6.26 Å), and SrF_2 (5.845 Å) are in a good agreement with experimental values 5.46 Å [69], 6.20 Å [70], and 5.799 Å [71], respectively.
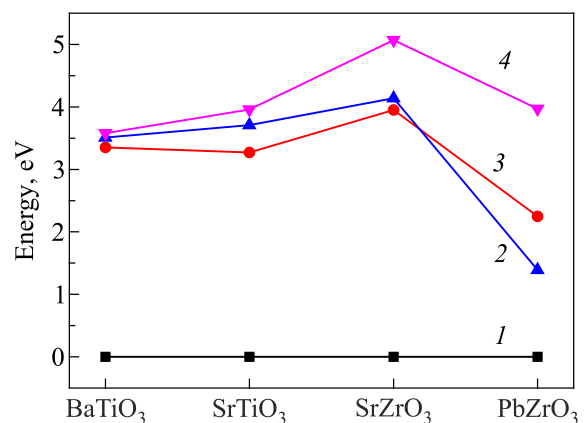
Fig. 5. *Ab initio* B3PW calculated $BaTiO_3$, $SrTiO_3$, $SrZrO_3$, and $PbZrO_3$ perovskite bulk (*3*) and (001) surface (*2*) F center induced defect levels under the respective perovskite conduction band bottom (*4*). Represents the top of the $BaTiO_3$, $SrTiO_3$, $SrZrO_3$ and $PbZrO_3$ perovskite valence bands (*1*).

As a next step, we have calculated the two nearest neighbor atom displacements surrounding the bulk F centers in CaF_2, BaF_2, and SrF_2 matrixes (Table 3). For example, in the CaF_2 crystal, the repulsions of the four nearest Ca atoms from the F center (fluorine vacancy) are small and equal to 0.15 % of the a, while the second-nearest-neighbor F atoms are attracted towards the F center by 0.28 % of the a. Our calculated atomic displacements around the bulk F center in BaF_2 are even smaller than in CaF_2. So, four nearest Ba atoms are repulsed from the BaF_2 bulk F center by a very small magnitude, only 0.03 % of the a, while the second nearest neighbor F atoms are attracted towards the fluorine vacancy by 0.23 % of the a. In SrF_2, four nearest to the bulk F center Sr atoms, just opposite to the CaF_2 and BaF_2, are attracted towards the fluorine vacancy, again, by a very small displacement magnitude, only 0.02 % of the a (Table 3). The attraction of the second nearest neighbor F atoms in the SrF_2 crystal towards the F center are 0.27 % of the a, namely, almost equal as in the CaF_2 and BaF_2 matrixes.

Table 3. *Ab initio* B3PW calculated atomic and electronic structure of the F centers in CaF_2, BaF_2, and SrF_2 crystals

Calculated bulk F center properties	CaF_2	BaF_2	SrF_2
Lattice constant, Å	5.50	6.26	5.845
A effective charge in perfect crystal	1.803e	1.845e	1.908e
B atom effective charge in perfect crystal	−0.902e	−0.923e	−0.954e
A atom relaxation, % of a	0.15	0.03	−0.02
B atom relaxation, % of a	−0.28	−0.23	−0.27
F center charge inside vacancy	−0.752e	−0.801e	−0.848e
F center under conduction band, eV	4.24	4.27	3.67
Calculated band gap with F center (Γ–Γ), eV	10.99	11.28	11.34
E_{form}, eV	7.87	7.82	10.33

Inside the bulk F center, or in another words fluorine vacancy, in the CaF_2, BaF_2, and SrF_2 crystals are located −0.752e, −0.801e, and −0.848e of additional charge, respectively (Table 3). It is worth to notice, that in all three CaF_2, BaF_2, and SrF_2 fluorites, the calculated effective atomic charges are very close to those expected in an ionic model (+2e and −1e, respectively). For example, the Ca and F effective charges are equal to +1.803e and −0.902e, respectively, in the CaF_2 matrix (Table 3). The B3PW calculated bulk F center formation energies for the CaF_2 (7.87 eV), BaF_2 (7.82 eV), and SrF_2 (10.33 eV) fluorites are in the energy range between 7.82 and 10.33 eV (Table 3).

Taking into account that the obtained values of the formation energy are less than the appropriate values of band gap energy E_g, it can be concluded that the data of these calculations confirm the exciton mechanism of the F center formation in these materials.

Our calculation results for the F center induced defect level in the CaF_2 band gap (Table 3 and Fig. 6) suggest a possible mechanism for explanation of the optical absorption in CaF_2 observed experimentally at 3.3 eV [72]. This experimentally observed optical absorption at 3.3 eV may correspond to the electron transition from our calculated F center ground state to the conduction band. According to our calculations, the F center ground state at the Γ-point is located 6.75 eV above the top of the valence band and 4.24 eV below the conduction band bottom (Table 3 and Fig. 6), which is close to 3.3 eV. Thereby, our calculated CaF_2 band gap (distance from the valence band top to the conduction band bottom) containing the F center at the Γ-point is equal to 10.99 eV (Table 3 and Fig. 6), which is in a fair agreement with the corresponding experimental CaF_2 band gap equal to 11.5–12.1 eV [64, 65].

Also in BaF_2 the situation is similar. Namely, the experimentally observed optical absorption band (2.04 eV [65]) may be due to the electron transfer from the F center ground state, according to our B3PW calculations located 7.01 eV above the valence band top (Table 3 and Fig. 6), to the conduction band bottom, located 4.27 eV above the F center ground state. Thereby, our B3PW calculated BaF_2 band gap at Γ-point containing the F center defect is equal to 11.28 eV (Table 3 and Fig. 6), which is in a good agreement with the experimentally determined BaF_2 band gap energy of 10.30–11.00 eV [64, 65].

Finally, according to the experiment by Cavenett *et al.* [72], performed at low temperature, equal to 4 K, the optical
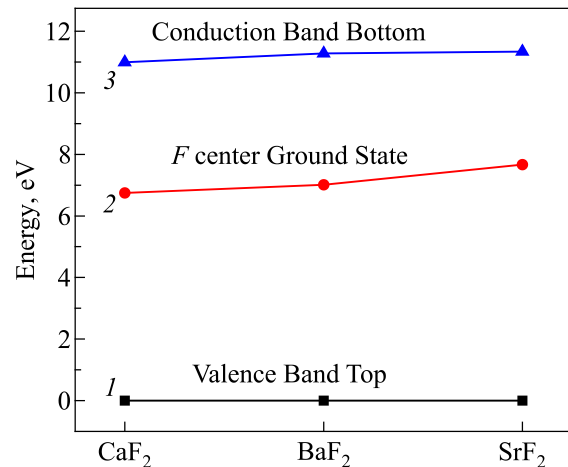
Fig. 6. Ab initio B3PW calculated CaF_2, BaF_2, and SrF_2 F center induced defect levels in the band gap (*2*). Represents the top of the CaF_2, BaF_2, and SrF_2 valence band (*1*). Represents the conduction band bottom (*3*).

absorption energy in a SrF_2 crystal with the F center is equal to 2.85 eV. According to our ab initio B3PW calculations (Table 3 and Fig. 6) the F center ground state is located 7.67 eV above the valence band top, or 3.67 eV below the conduction band bottom. So, the band gap containing the F center defect, according to our calculations, is equal to 11.34 eV, in an excellent agreement with the experimental value of 10.80–11.25 eV [64, 65]. Again, the experimentally observed F center absorption energy 2.85 eV [72] may be due to the electron transfer from the F center ground state located 7.67 eV above the valence band top to the conduction band bottom, located 3.67 eV higher.

Note that these calculations do not contradict the experimental facts about the possibility of the transition of an electron in the F center to an excited state, which, nevertheless, is in the band gap.

4. Conclusions

The nearest neighbor atomic displacement magnitudes in the ABO_3 perovskites typically are larger around the (001) surface than the bulk F centers. Moreover, the atomic displacement magnitudes around both bulk and (001) surface F centers in ABO_3 perovskites are considerably larger than the relevant atomic displacement magnitudes around the F center in CaF_2, BaF_2, and SrF_2 fluorites (Tables 1 and 3). It is worth to notice, that the nearest atom displacement magnitudes around the bulk F center in the CaF_2, BaF_2, and SrF_2 matrixes are very small and do not exceed 0.3 % of the lattice constant a.

In the ABO_3 perovskites, the charge always is considerably better localized inside the bulk F center than in the (001) surface F center (Table 2). Nevertheless, in ionic materials, like CaF_2, BaF_2, and SrF_2 the charge is much better localized inside the F center than in the ABO_3 perovskites. It is worth to mention, that around 80 % of the bulk F center charge is localized inside the fluorine vacancy in the CaF_2, BaF_2, and SrF_2 fluorites (Table 3).

In the $BaTiO_3$, $SrTiO_3$, and $SrZrO_3$ perovskites, the (001) surface F center induced defect levels in the perovskite band gap are located closer to the Conduction band bottom than for the respective bulk F centers (Table 2 and Fig. 5), indicating that both the bulk and (001) surface F centers are a shallow donor in the $BaTiO_3$, $SrTiO_3$, and $SrZrO_3$ perovskites (Fig. 5). The experimentally observed optical absorption in the CaF_2, BaF_2, and SrF_2 fluorites may correspond to an electron transition from the F center ground state, located in the CaF_2, BaF_2, and SrF_2 fluorite band gap, to the conduction band (Table 3 and Fig. 6).

The calculated formation energy difference between the $BaTiO_3$, $SrTiO_3$, $SrZrO_3$, and $PbZrO_3$ (Table 2 and Fig. 4) bulk and (001) surface F centers triggers the F center segregation from the bulk towards the ABO_3 perovskite (001) surfaces.

————

1. M. Dawber, K. M. Rabe, and J. F. Scott, *Rev. Mod. Phys.* **77**, 1083 (2005).

2. E. A. Kotomin, S. Piskunov, Y. F. Zhukovskii, R. I. Eglitis, A. Gopejenko, and D. E. Ellis, *Phys. Chem. Chem. Phys.* **10**, 4258 (2008).

3. V. Alexandrov, E. A. Kotomin, J. Maier, and R. A. Evarestov, *Eur. J. Phys. B* **72**, 53 (2009).

4. D. A. Carballo-Cordova, M. T. Ochoa-Lara, S. F. Olive-Mendez, and F. Espinoza-Magana, *Phil. Mag.* **99**, 181 (2019).

5. A. S. Farlenkov, A. G. Smolnikov, M. V. Ananyev, A. V. Khodimchuk, A. L. Buzlukov, A. V. Kuzmin, and N. M. Porotnikova, *Solid State Ion.* **306**, 82 (2017).

6. V. S. Vikhnin, H. M. Liu, W. Y. Jia, S. Kapphan, R. Eglitis, and D. Usvyat, *J. Lumin.* **83-84**, 109 (1999).

7. X. Jiao, T. Liu, Y. Lu, Q. Li, R. Guo, X. Wang, and X. Xu, *J. Electron. Mater.* **49**, 2137 (2020).

8. R. Merkle and J. Maier, *Angew. Chem. Int. Ed.* **47**, 3874 (2008).

9. S. A. Chambers, M. H. Engelhard, V. Shutthanandan, Z. Zhu, T. C. Droubay, L. Qiao, P. V. Sushko, T. Feng, H. D. Lee, T. Gustafsson, E. Garfunkel, A. B. Shah, J.-M. Zuo, and Q. M. Ramasse, *Surf. Sci. Rep.* **65**, 317 (2010).

10. R. Waser, R. Dittmann, G. Staikov, and K. Szot, *Adv. Mater.* **21**, 2632 (2009).

11. V. P. Savchyn, A. I. Popov, O. I. Aksimentyeva, H. Klym, Yu. Yu. Horbenko, V. Serga, A. Moskina, and I. Karbovnyk, *Fiz. Nizk. Temp.* **42**, 760 (2016) [*Low Temp. Phys.* **42**, 597 (2016)].

12. O. I. Aksimentyeva, V. P. Savchyn, V. P. Dyakonov, S. Piechota, Y. Y. Horbenko, I. Y. Opainych, P. Y. Demchenko, A. Popov, and H. Szymczak, *Mol. Cryst. Liq. Cryst.* **590**, 35 (2014).

13. D. Gryaznov, S. Baumann, E. A. Kotomin, and R. Merkle, *J. Phys. Chem. C* **118**, 29542 (2014).

14. H. Y. Su and K. Sun, *J. Mater. Sci.* **50**, 1701 (2015).

15. A. M. Deml, V. Stevanovich, A. M. Holder, M. Sanders, R. O. Hayre, and C. B. Musgrave, *Chem. Mater.* **26**, 6595 (2014).

16. D. Ricci, G. Bano, G. Pacchioni, and F. Illas, *Phys. Rev. B* **68**, 224105 (2003).

17. W. J. Yin, S. H. Wei, M. M. Al-Jassim, and Y. Yan, *Phys. Rev. B* **85**, 201201 (2012).

18. E. A. Kotomin and A. I. Popov, *Nucl. Instrum. Methods Phys. B* **141**, 1 (1998).

19. A. I. Popov, E. A. Kotomin, and J. Maier, *Nucl. Instrum. Methods Phys. B* **268**, 3084 (2010).

20. V. N. Kuzovkov, A. I. Popov, E. A. Kotomin, M. A. Monge, R. Gonzalez, and Y. Chen, *Phys. Rev. B* **64**, 064102 (2001).

21. A. Popov, M. Monge, R. Gonzalez, Y. Chen, and E. Kotomin, *Solid State Commun.* **118**, 163 (2001).

22. J. Carrasco, F. Illas, N. Lopez, E. A. Kotomin, Y. F. Zhukovskii, R. A. Evarestov, Y. Mastrikov, S. Piskunov, and J. Maier, *Phys. Rev. B* **73**, 064106 (2006).

23. A. I. Popov, E. A. Kotomin, and M. M. Kuklja, *Phys. Status Solidi B* **195**, 61 (1996).

24. E. A. Kotomin, R. I. Eglitis, and A. I. Popov, *J. Phys.: Condens. Matter* **9**, L315 (1997).

25. P. W. M. Jacobs, E. A. Kotomin, and R. I. Eglitis, *J. Phys.: Condens. Matter* **12**, 569 (2000).

26. R. I. Eglitis, E. A. Kotomin, G. Borstel, S. Kapphan, and V. S. Vikhnin, *Comput. Mater. Sci.* **27**, 81 (2003).

27. G. Borstel, R. I. Eglitis, E. A. Kotomin, and E. Heifets, *Phys. Status Solidi B* **236**, 253 (2003).

28. F. Karsai, P. Tiwald, R. Laskowski, F. Tran, D. Koller, S. Gräfe, J. Burgdörfer, L. Wirtz, and P. Blaha, *Phys. Rev. B* **89**, 125429 (2014).

29. J. Hoya, J. I. Laborde, D. Richard, and M. Renteria, *Comput. Mater. Sci.* **139**, 1 (2017).

30. A. F. Fix, F. U. Abuova, R. I. Eglitis, E. A. Kotomin, and A. T. Akilbekov, *Phys. Scr.* **86**, 035304 (2012).

31. N. Chuklina, S. Piskunov, N. V. Popov, A. Mysovsky, and A. I. Popov, *Nucl. Instr. Meth. B* **474**, 57 (2020).

32. A. Stashans and F. Vargas, *Mater. Lett.* **50**, 145 (2001).

33. J. Carrasco, F. Illas, N. Lopez, E. A. Kotomin, Yu. F. Zhukovskii, S. Piskunov, J. Maier, and K. Hermansson, *Phys. Status Solidi C* **2**, 153 (2005).

34. G. I. Meijer and T. H. Stöferle, *U.S. Patent No. 8,054,669*, U.S. Patent and Trademark Office (2011).

35. M. Arrigoni, E. Kotomin, D. Gryaznov, and J. Maier, *Phys. Status Solidi B* **252**, 139 (2015).

36. L. Weston, A. Janotti, X. Y. Cui, C. Stampfl, and C. G. Van de Walle, *Phys. Rev. B* **89**, 184109 (2014).

37. I. I. Leonidov, V. I. Tsidilkovski, E. S. Tropin, M. I. Vlasov, and L. P. Putilov, *Mater. Lett.* **212**, 336 (2018).

38. S. Piskunov, I. Isakoviča, and A. I. Popov, *Opt. Mater.* **85**, 162 (2018).

39. J. J. Brown, Z. Ke, W. Geng, and A. J. Page, *J. Phys. Chem. C* **122**, 14590 (2018).

40. M. Q. Cai, Y. J. Zhang, Z. Yin, and M. Zhang, *Phys. Rev. B* **72**, 075406 (2005).

41. M. Sokolov, R. I. Eglitis, S. Piskunov, and Y. F. Zhukovskii, *Int. J. Mod. Phys. B* **31**, 1750251 (2017).

42. M. Arrigoni, T. S. Bjornheim, E. Kotomin, and J. Maier, *Phys. Chem. Chem. Phys.* **18**, 9902 (2016).

43. R. I. Eglitis and A. I. Popov, *J. Nano-Electron. Phys.* **11**, 01001 (2019).

44. C. Duque and A. Stashans, *Physica B* **336**, 227 (2003).

45. R. I. Eglitis and S. Piskunov, *Comput. Condens. Matter* **7**, 1 (2016).

46. K. M. Eid and H. Y. Ammar, *Appl. Surf. Sci.* **257**, 6049 (2011).

47. B. G. Janesko and S. I. Jones, *Surf. Sci.* **659**, 9 (2017).

48. H. Häkkinen and M. Manninen, *J. Chem. Phys.* **105**, 10565 (1996).

49. G. Roy, G. Singh, and T. E. Gallon, *Surf. Sci.* **152-153**, 1042 (1985).

50. S. Folsch and M. Henzler, *Surf. Sci.* **247**, 269 (1991).

51. S. Folsch, A. Stock, and M. Henzler, *Surf. Sci.* **264**, 65 (1992).

52. M. Szymonski, J. Koloziej, P. Czuba, P. Piatkowski, and A. Poradzisz, *Phys. Rev. Lett.* **67**, 1906 (1991).

53. Z. Postawa, J. Kolodziej, G. Baran, P. Czuba, P. Piatkowski, M. Szymonski, I. Plavina, and A. Popov, *Nucl. Instrum. Methods Phys. B* **100**, 228 (1995).

54. V. Zielasek, T. Hildebrandt, and M. Henzler, *Phys. Rev. B* **62**, 2912 (2000).

55. V. Chakarian, T. D. Durbin, P. R. Varekamp, and J. A. Yarmoff, *Phys. Rev. B* **48**, 18332 (1993).

56. K. Schmalzl, D. Strauch, and H. Schrober, *Phys. Rev. B* **68**, 144301 (2003).

57. H. Shi, R. I. Eglitis, and G. Borstel, *Phys. Rev. B* **72**, 045109 (2005).

58. G. Fisicaro, M. Sicher, M. Amsler, S. Saha, L. Genovese, and S. Goedecker, *Phys. Rev. Mater.* **1**, 033609 (2017).

59. H. Shi, L. Chang, R. Jia, and R. I. Eglitis, *Comput. Mater. Sci.* **79**, 527 (2013).

60. H. Shi, L. Chang, R. Jia, and R. I. Eglitis, *J. Phys. Chem. C* **116**, 4832 (2012).

61. F. Tran and P. Blaha, *J. Phys. Chem. A* **121**, 3318 (2017).

62. H. Shi, R. Jia, and R. I. Eglitis, *Solid State Ion.* **187**, 1 (2011).

63. H. Shi, R. I. Eglitis, and G. Borstel, *J. Phys.: Condens. Matter* **18**, 8367 (2006).

64. G. W. Rubloff, *Phys. Rev. B* **5**, 662 (1972).

65. V. M. Lisitsyn, L. A. Lisitsyna, A. I. Popov, E. A. Kotomin, F. U. Abuova, A. Akilbekov, and J. Maier, *Nucl. Instrum. Methods Phys. B* **374**, 24 (2016).

66. A. D. Becke, *J. Chem. Phys.* **98**, 5648 (1993).

67. C. Lee, W. Yang, and R. G. Parr, *Phys. Rev. B* **37**, 785 (1988).

68. V. R. Saunders, R. Dovesi, C. Roetti, N. Causa, N. M. Harrison, R. Orlando, and C. M. Zicovich-Wilson, *CRYSTAL-2014 User Manual*, University of Torino, Italy (2014).

69. M. Nicolav, *J. Cryst. Growth* **218**, 62 (2000).

70. J. M. Leger, J. Haines, A. Atouf, and O. Schulte, *Phys. Rev. B* **52**, 13247 (1995).

71. W. Hayes, *Crystals with the Fluorite Structure*, Clarendon Press, Oxford (1974).

72. B. C. Cavenett, W. Hayes, I. C. Hunter, and A. M. Stoneham, *Proc. Royal Soc. A* **309**, 53 (1969).

F центри в об'ємі та на поверхні (001) оксидних перовскитів та фторидів лужноземельних металів: гібридні розрахунки з перших принципів методом Хартрі–Фока–DFT

R. Eglitis, A. I. Popov, J. Purans, Ran Jia

Представлено результати *ab initio* розрахунків та аналізу характеристик *F* центрів у об'ємі та на поверхні (001) оксидних перовскитів, таких як $BaTiO_3$, $SrTiO_3$, $SrZrO_3$, з подальшим їх порівнянням з *F* центрами у фторидах лужноземельних металів (CaF_2, BaF_2 та SrF_2). Виявлено, що у *F* центрах у перовскітах як в об'ємі, так і на поверхні (001), два найближчі до вакансії атома Ti або Zr взаємно відштовхуються, а наступні найближчі атоми О релаксують до кисневої вакансії. Встановлено, що отримані релаксації атомів у найближчому оточенні навколо *F* центру в перовскитах ABO_3 в цілому більші, ніж у фторидах лужноземельних металів. Основні стани об'ємного та (001) поверхневого *F* центрів у перовскитах $BaTiO_3$, $SrTiO_3$, $SrZrO_3$ знаходяться на 0,23, 0,69, 1,12 еВ та 0,07, 0,25, 0,93 еВ нижче за дно зони провідності, це вказує на те, що *F* центр є дрібним донором. Вакансії в $BaTiO_3$, $SrZrO_3$ та $PbZrO_3$ зайняті зарядами 1,103*e*, 1,25*e* та 0,68*e*, тоді як дещо менші заряди, 1,052*e*, 1,10*e* та 0,3*e*, локалізовані всередині *F* центру на поверхні (001) перовскита. На відміну від частково ковалентних перовскитів ABO_3, заряд добре локалізований (близько 80 %) всередині вакансій фтору в іонних фторидах CaF_2, BaF_2 та SrF_2.

Ключові слова: *Ab initio* розрахунки, *F* центр, перовскити.